A Kinetics and Modeling Study of RANTES(9−68) Binding to Heparin Reveals a Mechanism of Cooperative Oligomerization†

Romain R. Vivès,‡ Rabia Sadir,‡ Anne Imberty,§ Anna Rencurosi,§ and Hugues Lortat-Jacob*,‡

Institut de Biologie Structurale, CNRS-CEA-UJF, 41 rue Horowitz, 38027 Grenoble cedex 01, France, and Centre de Recherches sur les Macromolécules Végétales, CNRS (affiliated with Université Joseph Fourier), 38041 Grenoble cedex 09, France

Received July 16, 2002; Revised Manuscript Received October 10, 2002

ABSTRACT: Heparan sulfate (HS) and heparin bind to virtually all chemokines and have been shown to play critical roles in the regulation of their activities. However, both binding mechanisms and structural features involved in chemokine−HS interactions remain poorly defined. In the study presented here, we analyzed the binding of heparin to RANTES(9−68), a N-terminally truncated form of the CC-chemokine RANTES. Using biochemical and surface plasmon resonance (BIAcore system) approaches, we showed that the RANTES(9−68)−heparin interaction was characterized by a complex binding model that involved dimerization of the chemokine through a mechanism of positive cooperativity. Since RANTES(9−68) remains monomeric in solution, we concluded that heparin induced chemokine dimerization. The structure of a complex involving a RANTES dimer and a heparin heptadecasaccharide was proposed by molecular modeling. This model was used to design a dimer of "head to head" coupled octasaccharides that would fit the internal symmetry of the chemokine dimer. This engineered oligosaccharide bound RANTES(9−68) much better than a natural heparin fragment of the same length, further supporting the interaction process and the proposed structural model. Altogether, the data reported here provide a basis for understanding the mechanisms by which HS modulates RANTES functions.

Chemokines are a large family comprising more than 40 structurally related small cytokines. Two major classes of chemokines can be distinguished, on the basis of the first two conserved cysteine positions: the CC-group (with two adjacent cysteine residues) that comprises RANTES[1] (regulated on activation, normal T-cell expressed, and secreted), MCP-1 (monocyte chemoattractant protein-1), and MIP-1 (macrophage inflammatory peptides-1) and the CXC-group (two cysteines spaced by a single amino acid), which includes Il-8 (interleukin-8) and SDF-1 (stromal cell-derived factor-1).

Chemokines play key roles in many aspects of the immune and inflammatory responses, primarily by attracting and activating leukocytes (*1*−*4*). A growing amount of evidence suggests that these proteins also control a range of other functions that extend well beyond the mere regulation of leukocyte migration. These include events as diverse as development, angiogenesis, neuronal patterning, hematopoiesis, viral infection, wound healing, metastasis, or host defense mechanisms, such as adhesion, respiratory burst, and degranulation (*5*−*8*). Chemokine signaling is primarily dependent on binding to a family of cell surface seven-transmembrane-spanning, G-protein-coupled receptors, which triggers intracellular signal transduction events (*4*, *9*), such as calcium mobilization or phosphorylation of serine/threonine kinases. Like other cytokines and growth factors, signal transduction mediated by chemokines may require receptor dimerization (*10*, *11*). In vitro studies have shown considerable redundancy in this system, with several chemokines binding to a single receptor, and several receptors being recognized by the same ligand. Overlapping ligand specificities and broad expression patterns presumably contribute to the diversity of chemokine activities.

Another common aspect of chemokines is their ability to interact with glycosaminoglycans (GAGs), usually heparan sulfate (HS), and several lines of evidence point out the importance of HS in promoting chemokine activity. First, in vitro, almost all chemokines studied to date appear to bind HS, suggesting that this interaction represents a fundamental aspect of these proteins. Second, the finding that T-lymphocytes secrete CC-chemokines (including RANTES and MIP-1), in vivo, as a complex with proteoglycans strongly suggests that this form is physiologically relevant (*12*). Finally, from a functional point of view, it is believed that chemokine binding to cell surface HS of endothelial cells contributes to the establishment of chemotactic gradients, hence providing directional cues for migrating leukocytes

† This work was supported by the Agence Nationale pour la Recherche sur le SIDA (ANRS), Sidaction, the Fondation pour la Recherche Médicale (FRM), and the Centre National de la Recherche Scientifique (CNRS). A.R. is an EEC postdoctoral fellow (HPRN-CT2000-00001).

* To whom correspondence should be addressed: IBS/LBM, 41 rue Horowitz, 38027 Grenoble cedex 01, France. Telephone: (+33) 476 88 95 69. Fax: (+33) 476 88 54 94. E-mail: Hugues.Lortat-Jacob@ibs.fr.

‡ CNRS-CEA-UJF.

§ CNRS (affiliated with Université Joseph Fourier).

[1] Abbreviations: HS, heparan sulfate; RANTES, regulated on activation, normal T-cell expressed, and secreted; MCP-1, monocyte chemoattractant protein-1; MIP-1, macrophage inflammatory peptide-1; Il-8, interleukin-8; SDF-1, stromal cell-derived factor-1; dp, degree of polymerization.

10.1021/bi026459i CCC: $22.00
Published on Web 11/20/2002

(*13*). HS may also protect chemokines from proteolytic degradation and could induce chemokine oligomerization at the cell surface, thus promoting local high concentrations at the vicinity of the G-coupled signaling receptor (*14*).

Chemokines and chemokine receptors represent attractive targets for therapeutic intervention, in particular, during inflammatory diseases but also, since some of them have been recognized as coreceptors for the human immunodeficiency virus (HIV) entry, in viral infection (*5*, *15*). For example, SDF-1, which binds to CXCR4, inhibits the entry of HIV strains that use CXCR4 as a coreceptor (*16*), while the entry of CCR5 using HIV can be inhibited by RANTES (*5*). However, administration of chemokines for therapeutic purposes may be hampered by the numerous activities elicited by these powerful mediators.

On the basis of the observation that the biological activity of RANTES depends on the integrity of its N-terminal domain, truncated forms of the chemokine have been produced. Interestingly, engineered RANTES lacking the first eight N-terminal amino acids, termed RANTES(9−68), has been found to bind several CC-chemokine receptors, including CCR5, although with a lower affinity than wild-type RANTES, but lacks chemotactic and leukocyte activating properties. This truncated form of the chemokine inhibits HIV entry (*5*), indicating that signaling and antiviral activities can be uncoupled.

The importance of HS binding to RANTES, in particular for the chemokine antiviral activity, has been addressed in a number of studies, but quite conflicting results have been reported. It is generally recognized that cell surface HS promotes RANTES anti-HIV properties (*17*, *18*), probably by facilitating the interaction of the chemokine with the cell surface. However, soluble GAGs, which should compete with cell surface GAGs, have been shown to enhance the chemokine antiviral activity in some cell systems (*12*), but not in others (*18*). This discrepancy is likely to reflect differences in the various cell types that have been considered, particularly with regard to the nature and the expression levels of the GAGs at the surface of these cells. It has also been reported that RANTES in complex with soluble GAGs failed to activate CCR5 (no induction of intracellular Ca^{2+} mobilization) but still demonstrated suppressive activity against HIV-1, implying that GAGs allow binding of RANTES to the HIV-1 entry domain of CCR5, but prevent its interaction with determinants required for signaling activity (*19*). However, other studies demonstrated that soluble GAGs inhibited both CCR5 binding and functional response (*20*−*22*). Finally, high concentrations of RANTES are known to enhance viral infection in the presence of HS, an effect that has been attributed to the ability of the chemokine to oligomerize on GAGs and cross-link the virus to cells via GAGs present on the membrane of both virions and cells (*23*).

In this study, we defined further the structural and dynamic features of the RANTES−HS interaction using a number of approaches, including Biacore-based binding analyses, cross-linking strategies, and molecular modeling. To overcome methodological hurdles caused by the tendency of RANTES to self-aggregate, we used RANTES(9−68) which, in contrast to full-length RANTES, remains monomeric in solution (*24*). This enabled us to analyze the direct contribution of HS in chemokine dimerization. Our data provided a structural model that should help in the understanding of mechanisms by which GAGs modulate this chemokine activity.

EXPERIMENTAL PROCEDURES

Materials. An upgraded BIAcore 1000 instrument, an F1 sensorchip, an amine coupling kit, and HBS-EP buffer [10 mM HEPES, 150 mM NaCl, 3 mM EDTA, and 0.005% surfactant P20 (pH 7.4)] were purchased from Biacore AB. Heparin was obtained from Sigma. Size-defined heparin (9 kDa) was a kind gift of M. Petitou (Sanofi). Heparinase I (EC 4.2.2.7) and heparinase III (EC 4.2.2.8) enzymes were supplied by Grampian Enzymes. Bio-gel P10 was from Bio-Rad. The polyclonal anti-human RANTES goat antibody and the peroxidase-conjugated anti-goat rabbit antibody were from R&D systems and Interchim, respectively. [^{3}H]Glucosamine was from Amersham Pharmacia Biotech.

Preparation of Heparin Oligosaccharides. Heparin oligosaccharides were prepared as described previously (*25*). Briefly, porcine mucosal heparin (10 g) was digested by heparinase I (8 mIU/mL) in 5 mM Tris, 2 mM $CaCl_2$, 50 mM NaCl, and 0.1 mg/mL bovine serum albumin (pH 7.5) for 54 h at 25 °C. Enzyme digestion was stopped by heating the reaction mixture at 100 °C for 5 min. Digestion products were then separated by size, using a Bio-Gel P10 column (150 cm × 4.4 cm) equilibrated in 0.2 M NaCl and run at 1 mL/min. Elution of the material was monitored by the absorbance at 232 nm. Collected fractions corresponding to the apex of each size-defined peak were pooled, dialyzed against water, and freeze-dried, and samples were reanalyzed by gel chromatography. Purified oligosaccharides were quantified by the colorimetric assay (*26*), or weighed.

Linear Chemical Conjugation of Heparin-Derived Oligosaccharides. Preparation of coupled "head to head" oligosaccharides involved reduction with sodium cyanoborohydride ($NaCNBH_3$) of Schiff bases formed between the saccharide aldehyde groups (at the reducing ends) and the primary amines of ethylenediamine used as a linker. The reaction was performed in two steps, as this was shown to improve coupling yields (personal communication from C. Freeman, Australian National University, Canberra, Australia). Size-defined hexa- and octasaccharides (250 μg) were first incubated for 48 h at 60 °C with a 1000-fold molar excess of ethylenediamine and 100 mM $NaCNBH_3$. Reacted oligosaccharides were then separated from the reagent mixture by gel filtration on a PD-10 column and freeze-dried. These oligosaccharides were resuspended in 100 mM $NaCNBH_3$ toghether with a further 750 μg of the corresponding unmodified oligosaccharides and incubated for an additional 48 h at 60 °C. Coupled oligosaccharides (dp6−dp6 and dp8−dp8) were finally separated from noncoupled material (dp6 and dp8) on a P10 column (100 cm × 0.75 cm), equilibrated in 0.25 M ammonium bicarbonate, and run at 4 mL/h. Eluted material was monitored by the absorbance at 232 nm. Peaks of the dp6−dp6 and dp8−dp8 compounds eluted at the positions expected for dp12 and dp16, respectively. Corresponding fractions were pooled and freeze-dried several times to remove residual ammonium bicarbonate. Recovered material was quantified by measuring the absorbance at 232 nm, compared to standard curves established with each starting oligosaccharide (dp6 and dp8).

Preparation of ^{3}H-Labeled Heparan Sulfate Oligosaccharides. HS oligosaccharides from Chinese hamster ovary cells were prepared as described previously (*25*). Metabolic radiolabeling was performed by incubation of confluent cells for 48 h in Ham's culture medium devoid of glucose and supplemented with 10 μCi/mL of [^{3}H]glucosamine. Radiolabeled HS was extracted by DEAE-Sephacel chromatography, purified with chondroitinase ABC (1 unit/mL, 3 h at 37 °C) and papain (1 mg/mL, 16 h at 65 °C) digestion, and rechromatographed on the DEAE-Sephacel column. Intact HS chains were then digested with heparinase III (20 mIU/mL, 4 h at 30 °C), and the resultant oligosaccharides were separated by size, using a Bio-gel P10 column (150 cm × 1 cm) equilibrated in 0.2 M NaCl and run at 4 mL/h.

Kinetic Analysis of the Heparin−RANTES(9−68) Interaction by Surface Plasmon Resonance (SPR). Size-defined heparin (9 kDa) was biotinylated at the reducing end and immobilized on a BIAcore sensor chip as described previously (*25*). For binding assays, different RANTES(9−68) concentrations (ranging from 0 to 5 μg/mL, in HBS-EP buffer) were injected over the heparin surface for 4 min at a flow rate of 20−50 μL/min, followed by a 7 min washing step with HBS-EP buffer. Because the complexes dissociate easily, it was not necessary to include a regeneration step at the end of each cycle. In parallel experiments, the same RANTES concentrations were injected on a control surface that underwent exactly the same chemistry (EDC/NHS activation, streptavidin coupling, and ethanolamine blocking) except for functionalization with biotinylated heparin. Sensorgrams were analyzed using the BIAevaluation 3.0 software as described previously (*27*). For that purpose, both the entire injection phase and the entire dissociation phase of all the binding curves were selected and simultaneously fitted to different binding models. Equilibrium data were also extracted from the sensorgram at the end of each injection, and plotted according to the Scatchard representation. Because of the positive cooperativity mechanism it suggests (see the Results), data were also analyzed according to the theory of Hill, to calculate the index of cooperativity. Finally, binding isotherms were also fitted to a developed binding model (see the Results), using Mathematica.

Filter Binding Assay. To analyze the binding of oligosaccharides to proteins in solution, a modified version of the filter binding assay of Maccarana et al. (*28*) was used. Briefly, RANTES(9−68) (0.5 μg) and biotinylated heparin (0.1 μg/mL) were co-incubated for 2 h at room temperature in 200 μL of Tris-buffered saline (TBS). Competition assays were performed by adding unlabeled oligosaccharides to the mixture. RANTES(9−68) and any bound biotinylated heparin were then trapped on the surface of a nitrocellulose membrane by drawing the incubation mixture through the membrane with a vacuum-assisted dot-blot apparatus. The nitrocellulose membrane was washed twice with 200 μL of TBS and blocked with 5% dry milk in TBS containing 0.05% Tween 20. The biotinylated heparin bound to RANTES(9−68) was revealed by incubating the membrane with extravidin peroxidase (0.5 μg/mL) and enhanced chemiluminescence (ECL) detection reagents. The membrane was exposed to film, and chemiluminescent signals were quantified by densitometry. For the direct binding assay, RANTES(9−68) (1.5 μg) was incubated with ^{3}H-labeled HS oligosaccharides (10 000 cpm) and bound complexes were trapped on a nitrocellulose filter as described above. Protein-bound HS was then dissociated from the filter with 2 M NaCl and quantified by β-scintillation counting.

Covalent Cross-Linking of RANTES to Heparin Oligosaccharides. Covalent complexes between RANTES(9−68) and heparin oligosaccharides were formed using a two-step zero-length cross-linking procedure (*29*). Oligosaccharides (50 μg) were incubated with 6 mM EDC and 15 mM S-NHS in coupling buffer [100 mM MES and 100 mM NaCl (pH 6.0)] for 15 min at room temperature (RT). Free cross-linking reagents were inactivated by addition of β-mercaptoethanol (final concentration of 20 mM) and incubation for an additional 15 min. RANTES (2 μg) was added to aliquots of this oligosaccharide mixture and diluted with coupling buffer to obtain a RANTES:heparin molar ratio of 1:4, and the reaction mixture was left for 2 h at room temperature. Analysis of the reaction products was performed by SDS−PAGE (17% acrylamide) and Western blotting. The PVDF membrane was blocked overnight with TBS, 0.05% Tween 20, and 5% milk at 4 °C and incubated with the anti-RANTES antibody (2 μg/mL in TBS, 0.05% Tween 20, and 5% milk) for 1 h at room temperature. After being washed for 3 × 10 min with TBS and 0.05% Tween 20, the membrane was incubated with the peroxidase-conjugated secondary antibody (used at a 1:10000 dilution) for 1 h and then rinsed for an additional 3 × 10 min with TBS and 0.05% Tween 20. Bands were visualized by ECL.

Calculation of the RANTES Connolly Surface. Coordinates of the RANTES dimer were taken from the crystal structure of AOP-RANTES (*30*) [PDB entry 1B3A (*31*)]. The AOP group at the N-terminal end was replaced with a serine. All hydrogen atoms were added using the Sybyl molecular modeling package (*32*), and partial atomic charges were derived using the Pullman procedure. The positions of all hydrogen atoms were optimized with the Tripos force field (*33*). Connolly surfaces of the proteins were calculated using the MOLCAD program (*34*) from the Sybyl package.

Modeling the Heparin Chains. Different chain conformations of the heparin polysaccharide were generated. Chains of various lengths were built with alternating 2-N-sulfated, 6-O-sulfated α-D-Glc and 2-O-sulfated β-L-IdoA monosaccharides. The coordinates of the monosaccharides were taken from a databank of three-dimensional structures (http://infopc2.cermav.cnrs.fr/databank/monosaccharides/).

All of the glycosidic linkages were thought to be able to adopt two different conformations selected in the low-energy region of the Ramachandran-type (Φ and Ψ) energy maps previously published for these disaccharides or for closely related ones (*35*, *36*). With the torsional angles of the glycosidic linkage defined as $\Phi = \Theta$(O-5*i*−C-1*i*−O-1*i*−C-4*j*) and $\Psi = \Theta$(C-1*i*−O-1*i*−C-4*j*−C-5*j*), the following conformations were considered: α-D-Glc(1−4)β-L-IdoA(^2S_O) repeating unit, $\Phi = 80°$ and $\Psi = -160°$, and $\Phi = 130°$ and $\Psi = -100°$; α-D-Glc(1−4)β-L-IdoA($^1C_4$) repeating unit, $\Phi = 90°$ and $\Psi = -150°$, and $\Phi = 90°$ and $\Psi = -70°$; β-L-Ido(^2S_O)(1−4)α-D-GlcA repeating unit, $\Phi = -90°$ and $\Psi = 170°$, and $\Phi = -90°$ and $\Psi = -110°$; and β-L-Ido($^1C_4$)(1−4)α-D-GlcA repeating unit, $\Phi = -80°$ and $\Psi = -170°$, and $\Phi = -80°$ and $\Psi = -110°$. Several dozen chain conformations were generated by randomly selecting both the occurrence of ^2S_O and $^1C_4$ ring shapes for the iduronic acid and the conformational state of each glycosidic linkage.

Few conformations were rejected because of steric conflicts. Atom types and partial charges were defined according to the PIM energy parameters for carbohydrates (*37*) to be used within the Tripos force field (*33*).

Docking Procedure. The GRID program (*38*) was used to predict the most favorable anchoring position for a charged sulfate group at the surface of the RANTES dimer. The probe used in the calculation was the charged oxygen of a sulfate or phosphate group. The grid spacing was set to 1 Å. From our library of heparin chain conformations, those that displayed a shape appropriate for fitting their sulfate groups with the GRID lowest isoenergy contours were selected. The polysaccharide chains were merged with the protein structure in the docking mode that brings the sulfate in close contact with the protein surface without generating steric conflicts. The geometry of each of these complexes was optimized by several cycles of energy minimization. Hydrogen atoms and pendent groups were first optimized. Finally, the whole heparin moiety, together with the side chain of the amino acids in the positively charged area, was fully optimized. All energy calculations were performed with the Tripos force field (*33*) together with energy parameters specially derived for carbohydrates and sulfated derivatives (*37*).

The symmetric synthetic analogue (head to head linked oligosaccharides) was modeled, starting from two hexasaccharide fragments, using the molecular editor in the Sybyl program. Appropriate charges were assigned to the linker. A systematic search of the low-energy conformations of the linker was carried out while maintaining its 2-fold symmetry. Among the low-energy conformers, those adopting an S shape compatible with the RANTES binding site were docked on the binding site, by superimposing the axes of symmetry of the ligand and of the protein dimer. Energy minimization was run under the same conditions that were used for the heparin fragment ligand.

RESULTS

Size Requirements of Heparin Oligosaccharides for Binding to RANTES. Oligosaccharide size dependence for the binding of RANTES to heparin and to HS was investigated by two means. First, a range of sized oligosaccharides (from dp2 to dp18) was prepared by enzymatic (heparinase I) digestion of heparin and subsequent purification by gel chromatography. Such a procedure yielded a range of sized oligosaccharides, featuring a similar charge:length ratio (*39*). The ability of these oligosaccharides to compete against heparin for binding to RANTES(9−68) was investigated, using the BIAcore system. The chemokine was preincubated with various concentrations of oligosaccharides and injected onto the heparin surface. Reduction of the level of RANTES binding was monitored and provided an indication of the ability of each oligosaccharide to interact with the chemokine (Figure 1A). Fragments shorter than octasaccharides did not prevent the RANTES−heparin interaction, whereas a gradual, size-dependent reduction of RANTES amounts bound to the surface could be observed with oligosaccharides ranging from dp8 to dp18. Full-length heparin displayed a greater binding capacity than dp18, presumably because it contains a multiplicity of binding sites.

The other approach involved direct interaction assays, using filter binding analysis. For this purpose, sized oligosaccharides (from dp2 to dp18) were prepared by heparinase III digestion of CHO metabolically labeled HS. RANTES(9−68) was incubated with 10 000 cpm of each sized oligosaccharide sample, and applied to a nitrocellulose membrane. Free oligosaccharides were washed away, and then RANTES-bound oligosaccharides trapped on the membrane were eluted with 2 M NaCl. The amounts of recovered oligosaccharides were estimated by scintillation counting (Figure 1B). The extent of binding to RANTES(9−68) increased with oligosaccharide length, with threshold effects: no interaction observed with short oligosaccharides (dp2−dp6), weak binding for samples in the dp8−dp12 range, and, finally, significant and enhanced binding for fragments featuring at least 14 saccharide units. Although no plateau could be observed, the sigmoid shape of HS-bound amounts suggested that a dp18 is the oligosaccharide length necessary for maximum binding, in agreement with the results obtained in competition assays. Such a length could accommodate more than a single molecule of RANTES, suggesting that optimum binding occurs with oligomers of the chemokine (see below).

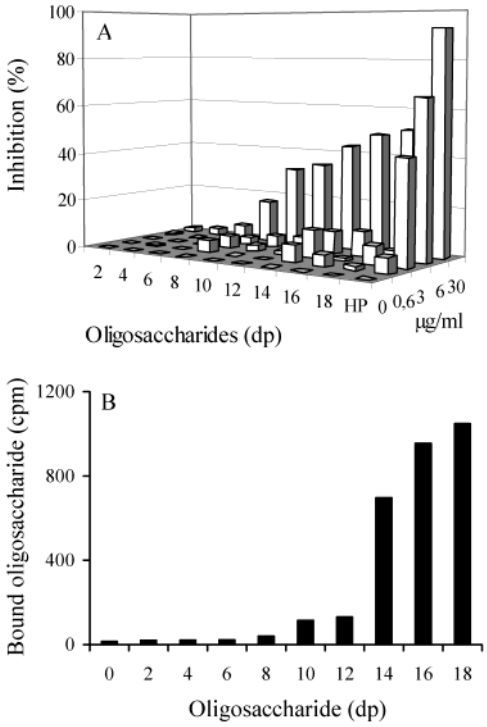

FIGURE 1: Binding of heparin−heparan sulfate fragments to RANTES(9−68). (A) Inhibition of RANTES binding to heparin. RANTES (1.5 μg/mL) was preincubated with various concentrations (0−30 μg/mL) of heparin (HP) or size-defined heparin oligosaccharides (dp2−dp18) and injected onto a heparin surface. The level of RANTES bound to the heparin surface at the end of the association phase was recorded and expressed as a percentage of inhibition. (B) Direct binding of HS to RANTES(9−68). RANTES (1.5 μg) was preincubated with 10 000 cpm of metabolically labeled HS oligosaccharides (dp2−dp18) and then dot-blotted onto a nitrocellulose membrane. RANTES-bound HS was quantified by scintillation counting.

Analysis of RANTES−Heparin Conjugates. To support the view that heparin-derived oligosaccharides contain more than one RANTES binding unit, the stable complex of an octadecasaccharide (dp18) with RANTES(9−68) was produced, using a two-step zero-length cross-linking procedure adapted to protein−GAG interaction studies (*29*, *40*). This

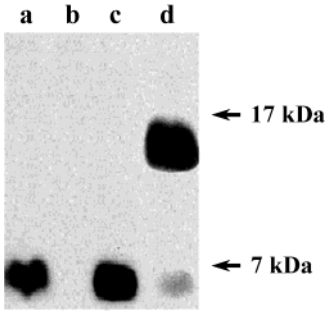

FIGURE 2: Analysis of RANTES−oligosaccharide cross-linking products. A heparin-derived octadecasaccharide was first activated by a mixture of EDC and NHS and then reacted with RANTES for 2 h. Cross-linked products were analyzed by 17% SDS−PAGE, followed by Western blotting: lane a, RANTES(9−68); lane b, activated heparin without RANTES(9−68); lane c, RANTES(9−68) and cross-linking reagents without heparin; and lane d, RANTES(9−68) cross-linked to the octadecasaccharide.

method enables specific cross-linking of heparin, or heparin-derived oligosaccharides within its actual binding site on RANTES(9−68), since no spacer is involved in covalent linkages between the polysaccharide carboxyl groups and the protein lysine residues. Moreover, this two-step procedure is designed to restrict activation by cross-linking reagents to the oligosaccharides only and, thus, does not allow protein−protein cross-linking (*29*).

Analysis of RANTES(9−68) by SDS−PAGE and Western blotting showed that it migrates as a single band with an apparent molecular mass of slightly les than 7 kDa (Figure 2, lane a) corresponding to a monomer of the protein. RANTES incubated with the cross-linking reagents also migrated as a single band of ∼7 kDa, showing that the protein was not cross-linked to itself, and remains monomeric in the absence of oligosaccharide (Figure 2, lane c). However, oligomerization of the chemokine was clearly induced by exposure to octadecasaccharide (dp18), the cross-linked product migrating with an apparent molecular mass of 15 kDa (Figure 2, lane d). Due to their high negative charge content, heparin fragments display very low apparent molecular masses compared to protein standards. With the conditions used for SDS−PAGE analysis (17% gels), dp18 runs slightly above the buffer front with an apparent molecular mass of approximately 1 kDa (data not shown). The apparent molecular mass of the RANTES−dp18 complex is thus consistent with a protein octadecasaccharide ratio of 2:1.

Binding of RANTES(9−68) to Sensorchip-Immobilized Heparin. A surface plasmon resonance binding assay, which we previously described for the CXC chemokine SDF-1 (*25*), was used to further analyze the heparin and heparan sulfate binding properties of RANTES(9−68). Typical sensorgrams were obtained by injection of a range of RANTES concentrations (50 to 625 nM) over the surface (Figure 3A). Injection of identical concentrations of RANTES over a control surface that underwent exactly the same chemistry (EDC/NHS activation, streptavidin coupling, and ethanolamine blocking), except for functionalization with biotinylated heparin, produced virtually no binding response (the maximum amount of binding was 5 RU with the highest RANTES concentration, data not shown). Visual inspection of the binding curves immediately showed that the chemokine associates at a high on-rate with heparin, equilibrium being

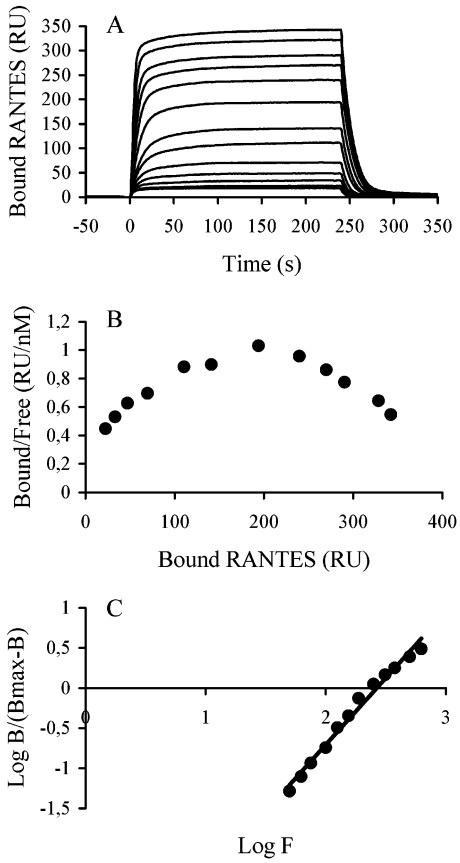

FIGURE 3: (A) Overlay of sensorgrams showing binding of RANTES(9−68) to heparin. RANTES at (from top to bottom) 625, 500, 375, 312.5, 200, 188, 156, 125, 100, 75, 62.5, and 50 nM was injected over a Biacore heparin surface at a flow rate of 50 μL/min for 4 min (0−240 s), after which running buffer was injected, and the response in RU was recorded as a function of time. (B) Scatchard plot of the equilibrium binding data directly measured on the sensorgrams at the end of the association phase. (C) Hill representation of the RANTES−heparin interaction. A function of the bound RANTES [log $B/(B_{max} - B)$] was plotted against the logarithmic concentration of the amount of injected RANTES (F). The slope provides an estimate of the Hill coefficient (n), and the intercept with the x-axis provides an estimate of the concentration of free RANTES required to occupy half of the binding sites.

reached in less than 1 or 2 min. Nevertheless, for equilibrium analysis, RANTES injections were carried out for at least 5 min. The formed complexes also spontaneously dissociate very rapidly from the surface, and binding curves returned to the baseline in less than 1 min with running buffer alone. Hence, it was not necessary to perform a regeneration step at the end of each cycle. To minimize all possible common artifacts, including mass transport and the rebinding effect, biotinylated heparin was immobilized to a low level (90 RU, 90 pg/mm^2), and the flow rate was maintained at 50 μL/min. Analysis of our data was performed on the entire time course of the reaction (including the whole association phase and the whole dissociation phase) using different binding models provided with the Biaevaluation 3.0 software. However, the binding curves could not be fitted in a satisfying manner to any of these binding models, suggesting a complex binding mode. To examine the RANTES−heparin interaction in more detail, the equilibrium data were first plotted according to the Scatchard representation. This yielded a curve with a convex shape, thus suggesting a

mechanism of positive cooperativity (Figure 3B). Accordingly, the Hill representation gave a straight line (Figure 3C), the intercept with the *X*-axis of which indicated that half-saturation occurs at 266 nM RANTES and the slope of which provided an estimate of the Hill coefficient (*n*). This coefficient equaled 1.66, confirming the positive cooperativity of this binding.

Binding of RANTES to Heparin Is a Two-Step Mechanism that Includes Dimerization and Positive Cooperativity. The data given above suggest that RANTES bound heparin as a dimer which encompasses 14−18 monosaccharides, and that the interaction appeared to be cooperative. Hence, a mathematical model was derived that would describe both these phenomena and to which our data could be fitted. First, we calculated that the fractional occupation of heparin ($y = [R]_{bound}/[H]_{total}$, where R is RANTES and H is heparin) has a maximum of approximately 4 (data from Figure 3A). Since the 9 kDa heparin was used (approximately 30 monosaccharides), this is in line with the occupation of 14−18 monosaccharides for a dimer of RANTES. The binding can thus be described as

$$H + R \leftrightarrow RH \quad (1)$$

$$RH + R \leftrightarrow R_2H \quad (2)$$

$$R_2H + R \leftrightarrow R_3H \quad (3)$$

$$R_3H + R \leftrightarrow R_4H \quad (4)$$

where

$$K_1 = [RH]/[R][H] \quad (5)$$

$$K_2 = [R_2H]/[RH][R] \quad (6)$$

$$K_3 = [R_3H]/[R_2H][R] \quad (7)$$

$$K_4 = [R_4H]/[R_3H][R] \quad (8)$$

K_1-K_4 being the equilibrium association constants of the four steps.

To introduce cooperativity into the model, a factor *f* was defined as

$$f = K_2/K_1 \quad (9)$$

If *f* is greater than 1, K_2 will be greater than K_1, meaning that the second RANTES binds heparin with a higher affinity than the first one. If a dimer corresponds to a binding unit, the binding of the third RANTES should not be influenced by the two first ones, yielding

$$K_3 = K_1 \quad (10)$$

$$K_4 = K_2 \quad (11)$$

The fractional occupation of heparin is

$$y = [R]_{bound}/[H]_{total} = ([RH] + 2[R_2H] + 3[R_3H] + 4[R_4H])/([H] + [RH] + [R_2H] + [R_3H] + [R_4H]) \quad (12)$$

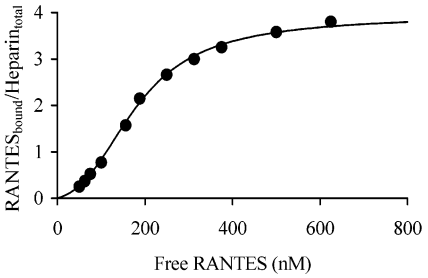

FIGURE 4: Nonlinear curve fitting of the equilibrium binding of RANTES to heparin. The fractional occupation of heparin by RANTES ($y = [RANTES]_{bound}/[heparin]_{total}$) was plotted against the concentration of free RANTES ($x = [RANTES]_{free}$), and the experimental data (●) were fitted to the developed binding model.

Introduction of eqs 5−11 into eq 12 leads to

$$y = [K_1x(1 + 2fK_1x + 3fK_1^2x^2 + 4f^2K_1^3x^3)]/[1 + K_1x(1 + fK_1x + fK_1^2x^2 + f^2K_1^3x^3)] \quad (13)$$

to which our data were fitted ($x = [R]$). Experimental data and a fitted curve, using eq 13, are shown in Figure 4. It indicates that the binding model developed above accurately describes the binding of RANTES to heparin [variance between experimental data and fitted curve (σ^2) equals 0.0034]. This analysis returned a K_1 value of 2.51×10^6 M^{-1}, and thus an affinity $1/K_1$ of 398 nM for the first RANTES molecule to be bound. The cooperativity factor *f* was found to be 4.74; hence, the second RANTES molecule binds to the preformed complex with an affinity $1/fK_1$ of 84 nM. This mathematical model thus further supports the heparin-induced dimerization of RANTES and indicates that 9 kDa heparin can accommodate two such dimers.

Properties of the RANTES Dimer Surface. Molecular modeling was used to describe the RANTES−heparin complex. For that purpose, the accessible surface of the RANTES dimer was calculated using the MOLCAD software (*34*), and color-coded according to the electrostatic potential (Figure 5A). The most positive area consists of the two bulbs created by the rather long loop connecting the third β-strand, and the C-terminal α-helix (Figure 5B), and is created by a cluster of three basic amino acids, Arg44, Lys45, and Arg47 (Figure 5C). This cluster constitutes a typical BBXB heparin binding site, and has been defined as the main site for heparin binding (*22*, *41*). Some basic amino acids on adjacent loops also participate in the establishment of the positive electrostatic potential in this area, particularly His23 and Lys25, which are located on the loop preceding the first β-strand.

Analysis of the accessible surface together with the electrostatic potential indicates therefore clearly which face of the protein dimer would be the best candidate for binding a negatively charged polysaccharide. To gain a finer analysis of the binding site for sulfated glycosaminoglycans, the GRID program was run, using a negatively charged oxygen as the probe for a sulfate group. The isoenergy contour corresponding to a low energy of interaction is superimposed on the Connolly surface in Figure 5A. A favorable area for binding sulfates appeared to be located in the middle of the positively charged bulbs, i.e., at the Arg44, Lys45, and Arg47 cluster but also in the valley between the two bulbs.

The prediction of binding sites for sulfate groups could be validated since sulfate ions, originating from the crystal-

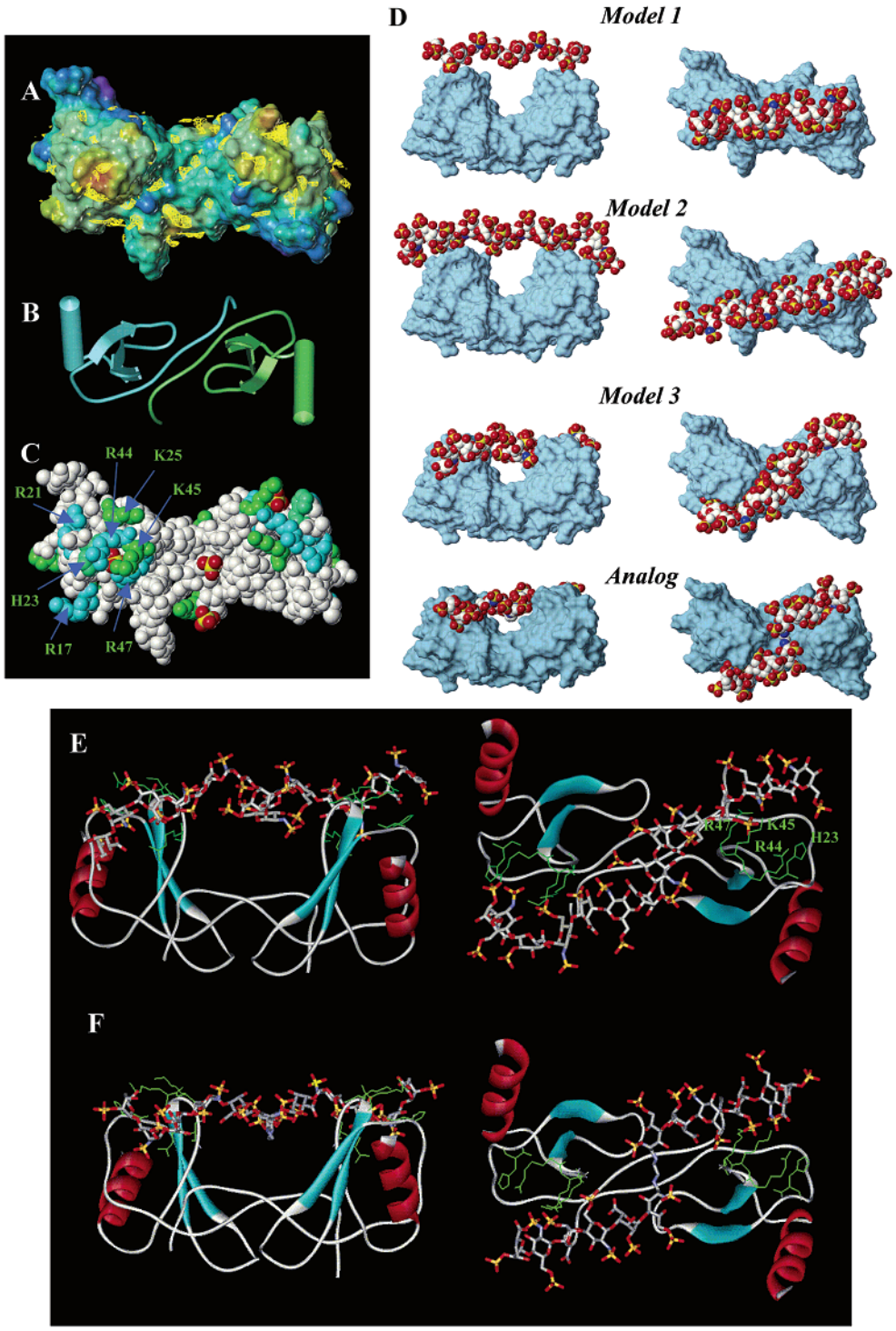

FIGURE 5: (A) Connolly surface of the RANTES dimer as calculated with the MOLCAD program. Surfaces are color-coded according to the electrostatic potential from blue (negative values) to red (positive values). Isoenergy contour for the best interaction of a charge negative oxygen (sulfate probe), as calculated with the GRID program superimposed on the Connolly surface. (B) Ribbon and tube representation of the dimer. (C) Space filling representation of the RANTES dimer together with the sulfate ions (yellow and red) observed in the crystal structure. Basic amino acids have been colored: Lys in green, Arg in cyan, and His in green-blue. (D) Representation of several low-energy RANTES−heparin complexes (models 1−3). The model of a complex consisting of a dimer of RANTES and a head to head linked dp6 is also shown (analog) with the same representation. Connolly surface and space filling representations have been used for the protein and the oligosaccharides, respectively. Hydrogen atoms are omitted. (E) Lowest-energy model for the interaction of the RANTES dimer with a heparin heptadecasaccharide. (F) Model for the interaction of the RANTES dimer with a head to head linked hexasaccharides. It shows that the head to head linked dp6 is a good mimic of natural heparin-derived oligosaccharides. In particular, the linker size almost exactly corresponds to the length of the protein central crevasse, enabling the two oligosaccharide fragments to interact optimally with the charged surfaces located on both sides of the protein. The protein is represented with a ribbon, except for the side chains of the basic amino acids directly involved in polysaccharide binding. The heparin molecule is represented with sticks. Hydrogen atoms are omitted.

lization buffer, have been observed in the crystal structures of AOP-RANTES (*30*) and Met-RANTES (*42*). Among the four sulfate ions cocrystallized with AOP-RANTES (Figure 5C), two are almost buried by the side chains of the Arg44,

Lys45, and Arg47 cluster, one is located in the cleft, and the other one is on the side of the molecule. The Met-RANTES crystal structure does not allow us to define additional sites since the two sulfate ions are located in positions identical to two of the ions cocrystallized with AOP-RANTES. Therefore, three of the four observed sulfate positions do correspond to binding regions predicted by our approach. In addition, a mutagenesis approach also pointed out the importance of Arg44, Lys45, and Arg47 for binding (*41*).

Molecular Modeling of the RANTES−Heparin Complex. The predicted binding site for sulfate ions, together with the location and shape of the positively charged area of the protein surface, served as the basis for docking several heparin fragments selected from a library of randomly generated conformations. Several binding modes allowed a close contact between the sulfated groups of heparin and the two positively charged bulbs of the protein surface. After optimization of the carbohydrate and protein side chain geometries, the interaction between the protein and the sugars was maximized. Figure 5D displays the three most interesting complexes in terms of energy and characteristics of the interaction. Model 1 displays the interaction between a linear and rather short (11 monomers) oligosaccharide. Stabilization of the complex is realized only by the sulfate groups at the extremity. In model 2, the oligosaccharide is longer (17 monomers) and adopts a bent shape that enables more extensive contacts with the two positively charged hills on the protein surface. The best energy of interaction is displayed in model 3, where the S shape of the heparin fragment allows interaction around each positively charged hill, rather than at their top. Furthermore, in this model the sulfate groups can interact strongly with the basic Arg44, Lys45, and Arg47 cluster (Figure 5E). For both monomers, one sulfate group from the oligosaccharide lies close to the observed sulfate ion location observed in the crystal structure.

Binding of RANTES to Head to Head Cross-Linked Oligosaccharides. To further support the positive cooperativity of the binding and molecular organization of the complex, a strategy was adopted in which oligosaccharides either monomeric or dimerized by chemical cross-linking competed with the binding of RANTES to heparin. We reasoned that if the two RANTES molecules bind to heparin independently of each other, this binding should be efficiently inhibited by an oligosaccharide with a length which just fit the binding site of one RANTES monomer (i.e., dp6 or dp8; see the model in Figure 5). On the other hand, if the two RANTES molecules of the complex depend on each other for binding to heparin, a molecule containing two binding sites (in the form of two cross-linked oligosaccharides) should have a better competitive activity than the same un-cross-linked oligosaccharide. Dimers of dp6 and dp8 were thus produced, using an original cross-linking strategy that allowed us to link two oligosaccharides, which, in addition, creates an internal symmetry that fits with the symmetry of the chemokine dimer. Results are shown in Figure 6A and indicate that cross-linking provides a very strong advantage over monomeric oligosaccharides that bind to the chemokine. In this assay, the molar amounts of monomeric oligosaccharides are twice that of cross-linked oligosaccharides; thus, the numbers of binding units are identical. Interestingly, cross-linked oligosaccharides (6−6 for instance; see Figure 6A) are even better competitors than monomeric un-cross-linked molecules having the same length (dp12 in this example). This could be due to the symmetry of the cross-linked oligosaccharides which fits with the symmetry of the chemokine dimer (schematic representation in Figure 6A). Alternatively, the spacer could provide increased flexibility and allow the two oligosaccharides to better interact with the protein. A model of the complex with the symmetric HS analogues (dp6−dp6) was built. It demonstrates that the linker size almost exactly corresponds to the length of the protein central crevasse, enabling the two oligosaccharide fragments to interact optimally with the charged surfaces located on both sides of the protein, rather than providing a degree of symmetry (see the analog panel of Figure 5D and Figure 5F). Finaly, we recently reported that the binding of heparin to stromal cell-derived factor-1α (SDF-1α), another

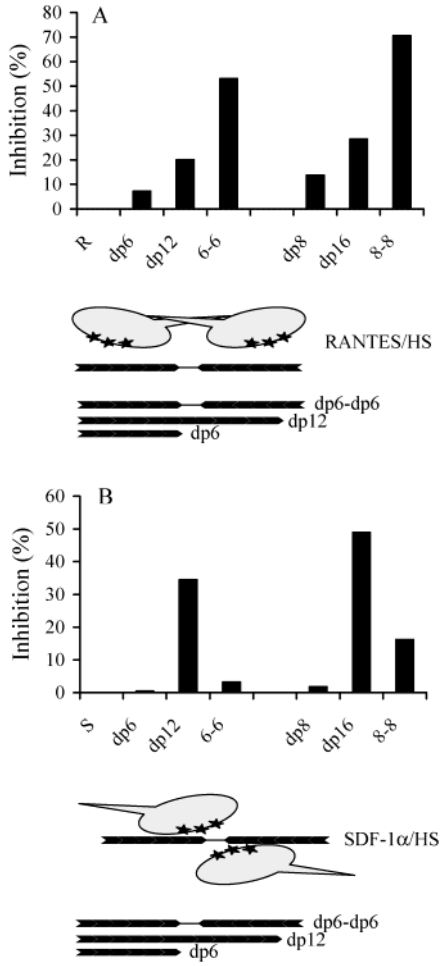

FIGURE 6: Binding of head to head cross-linked oligosaccharides to RANTES(9−68) and SDF-1α. Heparin-derived oligosaccharides prepared and cross-linked as described in Experimental Procedures were co-incubated at 10 μg/mL with RANTES (A) or SDF-1α (B) and then injected over a heparin surface. The amount of heparin-bound chemokine was recorded at the end of the injection and expressed as a percentage of inhibition. Oligosaccharides include hexasaccharide (dp6), octasaccharide (dp8), decasaccharide (dp12), hexadecasaccharide (dp16), cross-linked hexasaccharide (6−6), and cross-linked octasaccharide (8−8). R is RANTES without a competitor, and S is SDF-1α without a competitor. A schematic dimer of (A) RANTES and (B) SDF-1α bound to a cross-linked hexasaccharide is also displayed. On each chemokine, the binding residues are denoted with stars. Note that there are two distinct binding sites on the RANTES dimer, but only one at the protein−protein interface on the SDF-1α dimer.

chemokine, can be described as a one-step mechanism (*25*). In that case, the heparin binding site is located at the protein−protein interface, in the center of the chemokine dimer. As a "negative control", the experiments reported above were also repeated with SDF-1α. In contrast to what was observed with RANTES, cross-linked oligosaccharides did not compete much better than monomeric oligosaccharides and displayed an activity far below that of the molecules having the same length (Figure 6B and schematic representation).

DISCUSSION

It is widely appreciated that most chemokines, in addition to their cell surface receptors, bind to HS or other GAGs. Such interactions are of physiological relevance, as they presumably contribute to the formation of chemotactic gradients at the cell surface and in the extracellular matrices, which are essential for chemokine-mediated cell trafficking. A growing body of evidence also suggests that GAGs could facilitate the chemokine−receptor binding process by inducing structural changes such as oligomerization (*20*, *43*). Oligomerization is clearly important for RANTES, the aggregation state of which modulates its inflammatory activity as its ability to interfere with HIV infection (*44*, *45*). Oligomerization is believed to be promoted by GAGs (*14*); however, RANTES, like most chemokines, has the ability to self-aggregate in the absence of the polysaccharide (*46*). Hence, it is not really known if GAGs mediate oligomerization of chemokines or if oligomerization play a role in the ability of chemokines to interact with GAGs.

In the study presented here, we used a truncated form of the RANTES [RANTES(9−68)], which remains monomeric in solution (*24*, *47*). Using the Biacore system as a binding assay, we found that RANTES(9−68) displayed a high binding capacity for heparin. This is in agreement with the observation that the major heparin binding residues are located in the loop connecting the two strands [$\beta_{(2)}$ and $\beta_{(3)}$, residues 44−47 (*22*, *41*)], thus outside the removed first eight residues, but also indicates that monomeric RANTES still keeps its heparin binding ability. In contrast, we previously reported that the heparin binding amino acids of the CXC chemokine SDF-1α are located close to the protein−protein interface in the SDF-1α dimer, and that the functional binding site appears to be created by the dimerization of the protein (*25*).

The binding of RANTES(9−68) to heparin appears to strongly deviate from a simple one-to-one model. The complexity of the observed binding curves is due to the combination of two processes: oligomerization along the GAG chain and positive cooperativity. The fact that heparin can be loaded with several RANTES molecules does not necessarily imply protein−protein contact. However, analysis of the equilibrium data returned a Hill coefficient of 1.66, indicating that the binding of the different RANTES molecules depends on one another. A number of interactions characterized by such a Hill coefficient have been reported for dimerizing proteins, and these include the binding of MIP-1α to cellular HS (*14*). Curve fitting of the experimental data to binding models enabled us to propose that a first RANTES molecule associates with heparin with an affinity of 398 nM. This is followed by the binding of a second RANTES molecule that now displays an affinity of 84 nM. The enhanced affinity of the second RANTES molecule to be bound is presumably due to the fact that it binds both to heparin and to the first already bound RANTES, to form a dimer, consistent with the structural basis for homodimerization that exists for CC-chemokines. From a functional point of view, it is known that the RANTES receptor undergoes a ligand-mediated dimerization process required for Ca^{2+} flux and chemotaxis (*11*). However, it has been reported that the dimer dissociation constant for RANTES equals 35 μM (*48*). Although the RANTES concentration within tissues is difficult to evaluate, such a level might not be reached in vivo, and at a physiological concentration, full-length RANTES should be monomeric. In this context, it is thus possible that HS functions in promoting RANTES dimerization. Despite advances in the identification of chemokine receptor dimerization, the stoichiometry of the ligand receptor complex remains to be defined, and the possible role of HS in this process has been suggested (*49*). In the case of RANTES, dimerization has been difficult to study since full-length RANTES is partly or fully dimeric at concentrations used for biochemical and structural analyses. In this study, the use of RANTES(9−68), which remains monomeric even at high concentrations, enabled us to analyze the importance of heparin in mediating dimerization. Our data show that the binding of RANTES to heparin occurs in the nanomolar range, thus far below the dimer dissociation constant of RANTES alone (35 μM), and this may be a method of collecting and dimerizing RANTES at low and physiological concentrations.

Recent experiments have shown that HS synergizes with RANTES to inhibit HIV-1 replication in monocytes (*12*, *17*). It has also been shown that chemokine receptor dimerization, in that case CCR5, efficiently prevents HIV-1 infection (*50*). In that context, it is possible that one of the mechanisms by which HS synergizes with RANTES to inhibit HIV-1 infection is induction of CCR5 dimerization through HS-mediated RANTES dimerization. It is noteworthy that receptor activation requires residues near the N-terminus, while residues at positions 10−20 comprise another site that enables tight binding (*51*), two domains clearly outside the HS binding domain. Consequently, RANTES variants beginning with residue 6, 7, 8, 9, or 10, thus including RANTES-(9−68), bind to CCR5, without signaling (*52*). The use of RANTES(9−68) as a receptor antagonist to block HIV has been proposed (*5*). The present data on RANTES(9−68) dimerization therefore appear to be important for such a possibility.

Although we were unable, due to the complexity of the binding system, to derive the kinetic constants of this interaction, it is worth noting that the protein rapidly binds to and dissociates from heparin. This "dynamic" complex could reflect the fact that RANTES is immediately bound by HS within tissues, a point which is required for localization of the activity at the site of secretion, but also that it can rapidly be mobilized, for example, to extend the concentration gradient at the cell surface, and this can be another aspect of the functional importance of the RANTES−HS interaction.

Another point to be elucidated in the RANTES−heparin interaction was the size of the chemokine binding site on the polysaccharide. This was investigated using two approaches: competition assays for interaction with RANTES-

(9−68) between heparin and a range of size-defined heparin oligosaccharides and filter binding assays with HS-derived oligosaccharides extracted and purified from CHO cells. Both series of experiments gave very similar results and indicate an optimum length for the binding of dp16 to dp18, consistent with our molecular modeling approach. The fact that binding experiments performed with both heparan sulfate and heparin oligosaccharides yielded similar results with regard to optimal fragment size, despite differences in the sulfation levels of these two molecules, could suggest that structural motifs involved in RANTES binding may be restricted to a few sulfate groups and that variation in sulfation content mostly results in addition of redundant sulfates. Cross-linking of RANTES(9−68) to dp 18 showed the formation of a complex the apparent molecular mass of which is consistent with two RANTES molecules and the oligosaccharide, in agreement with the binding mechanism we proposed. HS consists of highly sulfated domains (S domains) with length and sequence diversity, spaced apart by slightly sulfated and flexible regions (*53*). The length and spacing of the S domains along the chain could be important in allowing the loading of monomeric or dimeric RANTES on the chain. To investigate this point, an original approach to coupling two oligosaccharides was designed. The resulting molecule consisted of two hexa- or octasaccharides linked by a spacer through their reducing end. Such an organization introduces an internal degree of flexibility and a 2-fold symmetry that fits the symmetry and organization of the protein dimer (*54*). These molecules have enhanced affinity for RANTES(9−68), compared to the equivalent heparin dodeca- or hexadecamer, thus validating our model. These data provide a clear indication of the overall structure of the RANTES binding motif on heparin, i.e., two short sulfated domains separated by a central region of least importance. This was further supported by the lack of activity of such compounds on SDF-1α, a chemokine which requires an uninterrupted central core within its binding sequence. Together, these results also support a recently published work based on molecular modeling studies (*55*), indicating that the required size and sulfation pattern of heparin fragments may differ for binding to different chemokines.

The chemical conjugation of defined heparin oligomers developed here should facilitate studies on HS domain structure and its importance for biological function, in particular, for homodimeric proteins that have an internal symmetry. Since this strategy is a two-step procedure, it is also possible to attach two different oligosaccharides (either in length or in sequence) that interact with two different proteins. For example, concomitant stimulation of cells with the chemokines RANTES and MCP-1 induces CCR5 and CCR2 receptor heterodimerization (*11*). The cross-linking strategy we describe here should be helpful in studying the role of HS in mediating such a process.

Finally, to further define the RANTES−heparin complex, the experimental data were combined with a molecular modeling approach, using the full-length RANTES dimer as a structural basis. In the RANTES−heparin complex, the polysaccharide is predicted to adopt an S shape that allows it to interact with the two positively charged bulbous regions present at the surface of the protein dimer, and which consists of typical BBXB heparin binding sites (residues 44−47). Some basic amino acids on adjacent loops also participate in the establishment of the positive electrostatic potential within this area, particularly His20 and Lys25, which are located on the loop preceding the first β-strand. An additional contact with heparin is established by His23 located in the loop connecting $\beta_{(N)}$ and $\beta_{(1)}$. Another sequence, KKWVR (residues 55−59), was initially proposed to act as a heparin binding site (*56*), but mutations within this cluster did not affect heparin binding (*41*). With regard to the orientation of both subunits in the RANTES dimer, bridging the two basic regions of each subunit (i.e., residues 44−47 and 55−59) with a single heparin chain could not be achieved. Our model is thus consistent with the view that the heparin binding site is composed of residues 44−47 of both units, and indeed does not support the presence of the second binding site. Our model also suggests that, along the chain, only a very small subset of sulfate groups is involved in the complex, a point consistent with the emerging view that within HS, unique sequences specifically bind a given ligand (*57*). As our comprehension of chemokine-induced receptor activation improves, these data should provide a basis for the understanding of how HS may modulate chemokine function. From a therapeutic point of view, the proposed model should also provide a structural framework for assisting the rational design of HS mimics which could modulate the formation of the RANTES−HS complex.

ACKNOWLEDGMENT

We thank Dr. Ian Clark-Lewis (University of British Columbia, Vancouver, BC) for his kind gift of RANTES-(9−68) and Eric Pellegrini (IBS, Grenoble, France) for the use of Mathematica.

REFERENCES

1. Baggiolini, M., Dewald, B., and Moser, B. (1997) *Annu. Rev. Immunol. 15*, 675−705.
2. Cyster, J. G. (1999) *Science 286*, 2098−2102.
3. Gale, L. M., and McColl, S. R. (1999) *BioEssays 21*, 17−28.
4. Rossi, D., and Zlotnik, A. (2000) *Annu. Rev. Immunol. 18*, 217−242.
5. Arenzana-Seisdedos, F., Virelizier, J. L., Rousset, D., Clark-Lewis, I., Loetscher, P., Moser, B., and Baggiolini, M. (1996) *Nature 383*, 400.
6. Zou, Y. R., Kottmann, A. H., Kuroda, M., Taniuchi, I., and Littman, D. R. (1998) *Nature 393*, 595−599.
7. Gerard, C., and Rollins, B. J. (2001) *Nat. Immunol. 2*, 108−115.
8. Muller, A., Homey, B., Soto, H., Ge, N., Catron, D., Buchanan, M. E., McClanahan, T., Murphy, E., Yuan, W., Wagner, S. N., Barrera, J. L., Mohar, A., Verastegui, E., and Zlotnik, A. (2001) *Nature 410*, 50−56.
9. Thelen, M. (2001) *Nat. Immunol. 2*, 129−134.
10. Vila-Coro, A. J., Rodriguez-Frade, J. M., Martin De Ana, A., Moreno-Ortiz, M. C., Martinez, A. C., and Mellado, M. (1999) *FASEB J. 13*, 1699−1710.
11. Mellado, M., Rodriguez-Frade, J. M., Vila-Coro, A. J., Fernandez, S., Martin de Ana, A., Jones, D. R., Toran, J. L., and Martinez, A. C. (2001) *EMBO J. 20*, 2497−2507.
12. Wagner, L., Yang, O. O., Garcia-Zepeda, E. A., Ge, Y., Kalams, S. A., Walker, B. D., Pasternack, M. S., and Luster, A. D. (1998) *Nature 391*, 908−911.
13. Sweeney, E. A., Lortat-Jacob, H., Priestley, G. V., Nakamoto, B., and Papayannopoulou, T. (2002) *Blood 99*, 44−51.
14. Hoogewerf, A. J., Kuschert, G. S., Proudfoot, A. E., Borlat, F., Clark-Lewis, I., Power, C. A., and Wells, T. N. (1997) *Biochemistry 36*, 13570−13578.
15. Schwarz, M. K., and Wells, T. N. (1999) *Curr. Opin. Chem. Biol. 3*, 407−417.
16. Oberlin, E., Amara, A., Bachelerie, F., Bessia, C., Virelizier, J. L., Arenzana-Seisdedos, F., Schwartz, O., Heard, J. M., Clark-

Lewis, I., Legler, D. F., Loetscher, M., Baggiolini, M., and Moser, B. (1996) *Nature 382*, 833−835.
17. Oravecz, T., Pall, M., Wang, J., Roderiquez, G., Ditto, M., and Norcross, M. A. (1997) *J. Immunol. 159*, 4587−4592.
18. Ylisastigui, L., Bakri, Y., Amzazi, S., Gluckman, J. C., and Benjouad, A. (2000) *Virology 278*, 412−422.
19. Burns, J. M., Lewis, G. K., and DeVico, A. L. (1999) *Proc. Natl. Acad. Sci. U.S.A. 96*, 14499−14504.
20. Kuschert, G. S., Coulin, F., Power, C. A., Proudfoot, A. E., Hubbard, R. E., Hoogewerf, A. J., and Wells, T. N. (1999) *Biochemistry 38*, 12959−12968.
21. Ali, S., Palmer, A. C., Banerjee, B., Fritchley, S. J., and Kirby, J. A. (2000) *J. Biol. Chem. 275*, 11721−11727.
22. Martin, L., Blanpain, C., Garnier, P., Wittamer, V., Parmentier, M., and Vita, C. (2001) *Biochemistry 40*, 6303−6318.
23. Trkola, A., Gordon, C., Matthews, J., Maxwell, E., Ketas, T., Czaplewski, L., Proudfoot, A. E., and Moore, J. P. (1999) *J. Virol. 73*, 6370−6379.
24. Ylisastigui, L., Vizzavona, J., Drakopoulou, E., Paindavoine, P., Calvo, C. F., Parmentier, M., Gluckman, J. C., Vita, C., and Benjouad, A. (1998) *AIDS 12*, 977−984.
25. Sadir, R., Baleux, F., Grosdidier, A., Imberty, A., and Lortat-Jacob, H. (2001) *J. Biol. Chem. 276*, 8288−8296.
26. Bitter, T., and Muir, H. (1962) *Anal. Biochem. 4*, 330−334.
27. Sadir, R., Forest, E., and Lortat-Jacob, H. (1998) *J. Biol. Chem. 273*, 10919−10925.
28. Maccarana, M., and Lindahl, U. (1993) *Glycobiology 3*, 271−277.
29. Pye, D. A., and Gallagher, J. T. (1999) *J. Biol. Chem. 274*, 13456−13461.
30. Wilken, J., Hoover, D., Thompson, D. A., Barlow, P. N., McSparron, H., Picard, L., Wlodawer, A., Lubkowski, J., and Kent, S. B. (1999) *Chem. Biol. 6*, 43−51.
31. Berman, H. M., Westbrook, J., Feng, Z., Gilliland, G., Bhat, T. N., Weissig, H., Shindyalov, I. N., and Bourne, P. E. (2000) *Nucleic Acids Res. 28*, 235−242.
32. Tripos Inc. (1998) *Sybyl*, St. Louis, MO.
33. Clark, M., Cramer, R. D. I., and van den Opdenbosch, N. (1989) *J. Comput. Chem. 8*, 982−1012.
34. Waldherr-Teschner, M., Goetze, T., Heiden, W., Knoblauch, M., Vollhardt, H., and Brickmann, J. (1992) in *Advances in Scientific Visualization* (Post, F. H., and Hin, A. J. S., Eds.) pp 58−67, Springer, Heidelberg.
35. Cros, S., Petitou, M., Sizun, P., Pérez, S., and Imberty, A. (1997) *Bioorg. Med. Chem. 5*, 1301−1309.
36. Mikhailov, D., Linhardt, R. J., and Mayo, K. H. (1997) *Biochem. J. 328*, 51−61.
37. Imberty, A., Bettler, E., Karababa, M., Mazeau, K., Petrova, P., and Pérez, S. (1999) in *Perspectives in Structural Biology* (Vijayan, M., Yathindra, N., and Kolaskar, A. S., Eds.) pp 392−409, Indian Academy of Sciences and Universities Press, Hyderabad, India.
38. Goodford, P. J. (1985) *J. Med. Chem. 28*, 849−857.
39. Ernst, S., Langer, R., Cooney, C. L., and Sasisekharan, R. (1995) *Crit. Rev. Biochem. Mol. Biol. 30*, 387−444.
40. Lortat-Jacob, H., Turnbull, J. E., and Grimaud, J. A. (1995) *Biochem. J. 310*, 497−505.
41. Proudfoot, A. E. I., Fritchley, S., Borlat, F., Shaw, J. P., Vilbois, F., Zwahlen, C., Trkola, A., Marchant, D., Clapham, P. R., and Wells, T. N. C. (2001) *J. Biol. Chem. 276*, 10620−10626.
42. Hoover, D. M., Shaw, J., Gryczynski, Z., Proudfoot, A. E. I., and Wells, T. (2000) *Protein Pept. Lett. 7*, 200.
43. Wells, T. N., Power, C. A., and Proudfoot, A. E. (1998) *Trends Pharmacol. Sci. 19*, 376−380.
44. Appay, V., Brown, A., Cribbes, S., Randle, E., and Czaplewski, L. G. (1999) *J. Biol. Chem. 274*, 27505−27512.
45. Appay, V., and Rowland-Jones, S. L. (2001) *Trends Immunol. 22*, 83−87.
46. Czaplewski, L. G., McKeating, J., Craven, C. J., Higgins, L. D., Appay, V., Brown, A., Dudgeon, T., Howard, L. A., Meyers, T., Owen, J., Palan, S. R., Tan, P., Wilson, G., Woods, N. R., Heyworth, C. M., Lord, B. I., Brotherton, D., Christison, R., Craig, S., Cribbes, S., Edwards, R. M., Evans, S. J., Gilbert, R., Morgan, P., and Hunter, M. G. (1999) *J. Biol. Chem. 274*, 16077−16084.
47. Laurence, J. S., LiWang, A. C., and LiWang, P. J. (1998) *Biochemistry 37*, 9346−9354.
48. Skelton, N. J., Aspiras, F., Ogez, J., and Schall, T. J. (1995) *Biochemistry 34*, 5329−5342.
49. Rodriguez-Frade, J. M., Mellado, M., and Martinez, A. C. (2001) *Trends Immunol. 22*, 612−617.
50. Vila-Coro, A. J., Mellado, M., Martin de Ana, A., Lucas, P., del Real, G., Martinez, A. C., and Rodriguez-Frade, J. M. (2000) *Proc. Natl. Acad. Sci. U.S.A. 97*, 3388−3393.
51. Pakianathan, D. R., Kuta, E. G., Artis, D. R., Skelton, N. J., and Hebert, C. A. (1997) *Biochemistry 36*, 9642−9648.
52. Gong, J. H., Uguccioni, M., Dewald, B., Baggiolini, M., and Clark-Lewis, I. (1996) *J. Biol. Chem. 271*, 10521−10527.
53. Gallagher, J. T. (2001) *J. Clin. Invest. 108*, 357−361.
54. Chung, C. W., Cooke, R. M., Proudfoot, A. E., and Wells, T. N. (1995) *Biochemistry 34*, 9307−9314.
55. Lortat-Jacob, H., Grosdidier, A., and Imberty, A. (2002) *Proc. Natl. Acad. Sci. U.S.A. 99*, 1229−1234.
56. Burns, J. M., Gallo, R. C., DeVico, A. L., and Lewis, G. K. (1998) *J. Exp. Med. 188*, 1917−1927.
57. Esko, J. D., and Lindahl, U. (2001) *J. Clin. Invest. 108*, 169−173.

BI026459I